LOW TEMPERATURE LUMINESCENCE OF RbCl:OH

A Thesis

Submitted to

the Faculty of Graduate Studies

In Partial Fulfillment

of the Requirements for the Degree

Master of Science

by

Ronald E. Silver

May 1971

ACKNOWLEDGEMENTS

The author wishes to thank Dr. I. Cooke for his supervision and help during the course of this study. Thanks is also extended to Dr. W. R. Wall for his assistance and many helpful suggestions. Help has also been given by Mr. P. Chaddock and Mr. A. McIlwain.

This research was supported by Defence Research Board and National Research Council.

TABLE OF CONTENTS

LIST OF FIGURES

LIST OF TABLES

ABSTRACT

Ultraviolet induced luminescence has been observed in a single crystal of rubidium chloride doped with a concentration of hydroxyl ions. The energies of the three emission bands found were shown to agree with previous results reported on the uv luminescence of similar crystals. Since the excitation spectra for the three emission bands were similar, the emission bands were interpreted as being due to transitions from the first electronic excited state to the first and second vibrational states of the ground electronic state.

The width of the main emission band as a function of temperature was investigated. This showed agreement with the functional variation predicted by the configurational coordinate model, yielding the phonon frequency and width at $0^{\circ}K$.

The difference of 0.04 ev between the first vibrational energy and the infrared OH^{-} stretching energy suggests that the vibrational states of the ground electronic state are described in the configurational coordinate model by parabolas with different parabolic constants than the ground electronic state.

CHAPTER I

INTRODUCTION

As early as 1940, an unidentified ultraviolet absorption band in KCl was observed by Aksinar at 203.4 nm.[1] It wasn't until much later that this band was identified as the absorption band due to OH^- centres. In 1958, two papers reported that the bands at 185 nm in NaCl, 204 nm in KCl and 214 nm in KBr were due to the OH^- centre.[20,21] In addition, Fritz et al[22] produced KCl crystals with varying OH^- concentrations as determined by the infrared band at 2.8 μ and showed that the 204 nm absorption band correlated with the OH^- concentration.

The hydroxyl ion is a very persistant impurity in air-grown alkali halides. Klein et al[2] showed that nominally pure alkali halide crystals bought from crystal manufacturers contained 1.4 parts per million mole fraction of OH^-. He showed that even when crystals were grown from reagent grade KCl after 12 hours of treatment with Cl_2 gas the mole fraction of OH^- was 0.1 ppm. This was also found by other researchers in conjunction with other studies.[3,4,5,6,7]

It has been shown by various methods that the OH^- dipole is substitutional and aligned with its axis along the [100] direction in alkali halide crystals. Kuhn and Lüty studying the paraelectric behavior of KCl concluded that the OH^- dipole has a potential minimum for orientations in the [100] direction.[9] Paus and Lüty from measurements of the density and lattice parameter change due to OH^- in KCl estimated that the potential barrier preventing the OH^- orientation in other than [100] directions is less than 4×10^{-2} ev.[10] This means that

at room temperature the OH^- ion would be in a state of free rotation. Stress dichroism studies in KCl have also shown that the orientation in [100] direction causes the expected splitting of the dipole degenerate ground state to be maximum for uniaxial stress in [100] direction reduced by a factor of $1/\sqrt{2}$ for [110] stress and zero for [111] stress.[11] Wedding and Klein[12] have determined the depth of the potential wells in the [100] direction for several alkali-halide lattices by measuring vibrational and librational modes of an OH^- doped crystal.

Because of the orientation along [100] directions Kuhn and Lüty concluded that it should be possible to produce paraelectric heating and cooling of a crystal.[9] This was observed experimentally by Känzig et al[13] and later by Kuhn and Lüty.[14] Shepherd reported that the electro-caloric effect can be used to cool a KCl crystal down to 0.36° from $1.3^{\circ}K$.[26] Stress on OH^- doped crystals is also reported to cause cooling.[11,16]

Bron and Dreyfus used microwave absorption and infrared absorption measurements to show that the OH^- centre of mass in KCl must be displaced by 0.3A from the halogen ion lattice site.[17] This agrees quite well with a displacement of 0.25A reported by Lawless.[16] Köstlin found that after lengthy irradiation of KBr:OH^- with uv at $80^{\circ}K$, U_2 centres (interstitial H atoms) were formed.[18] By taking linear warm up runs he established that the thermoluminescence was strictly proportional to the U_2 centre density. Thus he concluded that the OH^- centres are converted to O^{-2} and interstitial H atoms by uv irradiation.

A great deal of work has been done on the uv and infrared absorption spectra of OH^- ions in alkali halide lattices. Many researchers have reported that the OH^- concentration in alkali halide crystals is directly proportional to the infrared and uv absorption band strengths in the various alkali halides.[2,10,14,19] Klein et al correlated the area under the uv ab-

sorption band and the CH^- concentration as determined by pH titration measurements.[2] The conversion factors so calculated were applied to uv measurements for nominally pure alkali halide crystals to yield the approximate hydroxyl ion concentrations. Wedding and Klein used infrared absorption to investigate the main OH^- stretching band and its immediate side bands.[8]

Little work has been done on the luminescence of alkali halides containing hydroxyl impurities. In 1965, Köstlin[18] reported on the luminescence of $KBr:CH^-$. He found an emission peak broadening temperature dependence of $(\coth \frac{h\nu}{2kT})^{\frac{1}{2}}$. At the same time, Patterson and Kabler[23] correlated the uv emission with the IR absorption peak in $KBr:CH^-$. In 1967 Köstlin found that at low temperatures the emission spectra from $RbCl:CH^-$, $KI:CH^-$, $KBr:CH^-$ and $KCl:CH^-$ each resolved into a series of bands.[24] He noted that the energy separation between these bands corresponded to the vibrational energies reported in infrared absorption experiments. He found three such bands in KI and RbCl, four in KBr and seven in KCl.

The purpose of the present investigation is to duplicate the work of Köstlin[24] by measuring the energies of the three uv emission bands he reported for RbCl:OH, and extend this to determine the nature of the temperature dependence of the luminescence.

For later comparison it would be worthwhile to summarize the previous results obtained for RbCl:OH. Klein found from infrared absorption that the main vibrational energy was 3632.5 cm^{-1} or .450 ev.[8] The uv absorption peak and half width were measured at room temperature to be 5.78 ev or 215 nm and .66 ev or 24.5 nm respectively.[2] Köstlin found three emission peaks for $RbCl:CH^-$ with energies of 4.09, 3.68 and 3.28 ev.[24] He found that the uv absorption peak energy he measured agreed with the value reported by Klein.

CHAPTER II

EXPERIMENTAL METHOD

Photoelectron Pulse Counting

Light intensity measurement utilizing a photomultiplier can be accomplished with one of two methods:

1. By integrating the anode pulses which are generated from the photoelectrons created for each photon which strikes the cathode. The integration is done by shunting a high impedence voltmeter with a large resistor (between 100 KΩ and 10 MΩ) and a capacitor (approximately 1 μf). The measurement of the light intensity is then taken from the voltage measured on the voltmeter.

2. By counting the anode pulses with a scaler or multichannel analyser, (MCA). The pulses from the anode are first amplified and then analysed in a single channel analyser (SCA) which emits a logic pulse if the anode pulse height is between the upper and lower discrimination setting.

The anode signal measured for no incident light on the photomultiplier is called the dark current. The dark current must be taken into account in an intensity measurement. When the anode pulses are integrated the dark current can only be reduced by cooling the photomultiplier since this reduces the number of thermal electrons.

Some sources of dark current generate small pulses. These are ohmic leakage between the anode and adjacent elements, cold emission from the electrodes, and secondary electrons released by ionic bombardment of the dynodes.

Ionic bombardment of the cathode and residual radioactivity which produce photoelectron are sources of dark current which produce large pulses. Thus it is possible to reduce the dark current with photoelectron counting by using the SCA to remove the pulses with lower or higher pulse heights than the pulses produced by a light signal. The dark current pulse height spectrum of the photomultiplier used for all measurements in this investigation (EMI 6256S) is shown in figure 1, as measured by the MCA. This figure also shows the pulse height spectrum with a small light leak, and the pulse height spectrum due to only the light leak (i.e. with the dark current spectrum subtacted). Setting the SCA to trigger only for pulses with heights above channel 31 (.75V) reduces the dark current by a factor of 2.4. With photoelectron pulse counting the fractional statistical error associated with an intensity measurement can be reduced by counting for a longer time, since the absolute statistical error is the square root of the number of counts. Thus more accurate intensity measurements can be made by counting for a longer period of time, provided that there is sufficient temperature and light intensity stability. The error in integrating the photoelectron pulses is also limited by statistics. Increasing the resistance and capacitance increases the integrating time constant and thus the statistical error is decreased. However an approximate upper limit to the sizes of the resistance and capacitance is 10^7 ohms and 1 μf which gives a time constant of 10 seconds.

Figure 2 shows the integrated pulse measurement versus the photoelectron counting measurement for a range of incident intensities. This figure shows that for intensities below the intensity corresponding to 6.5 volts or 5,200 counts per second the two methods are linearly related. Above this intensity the greatest drawback of the photoelectron counting method shows

Figure 1

Pulse height spectrum of the photoelectric anode pulses from an EMI 6256S photomultiplier

(a) Dark current
(b) Small light leak with dark current subtracted
(c) Small light leak
(d) Large light leak with dark current subtracted
(e) Large light leak

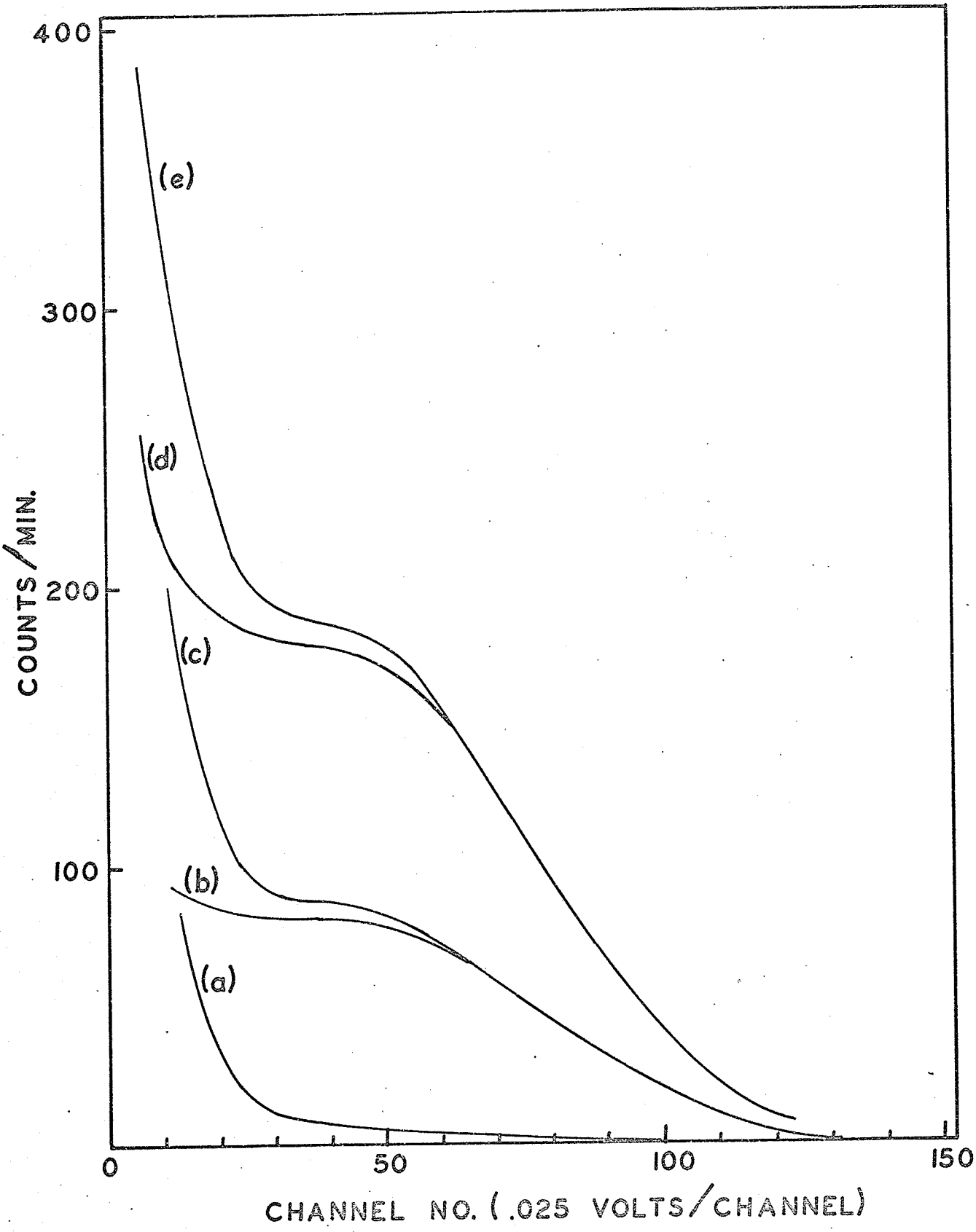
400
300
200
100
COUNTS / MIN.
(e)
(d)
(c)
(b)
(a)
0
50
100
150
CHANNEL NO. (.025 VOLTS/CHANNEL)

Figure 2

Photoelectron pulse counting measurement compared with the anode pulse integration measurement

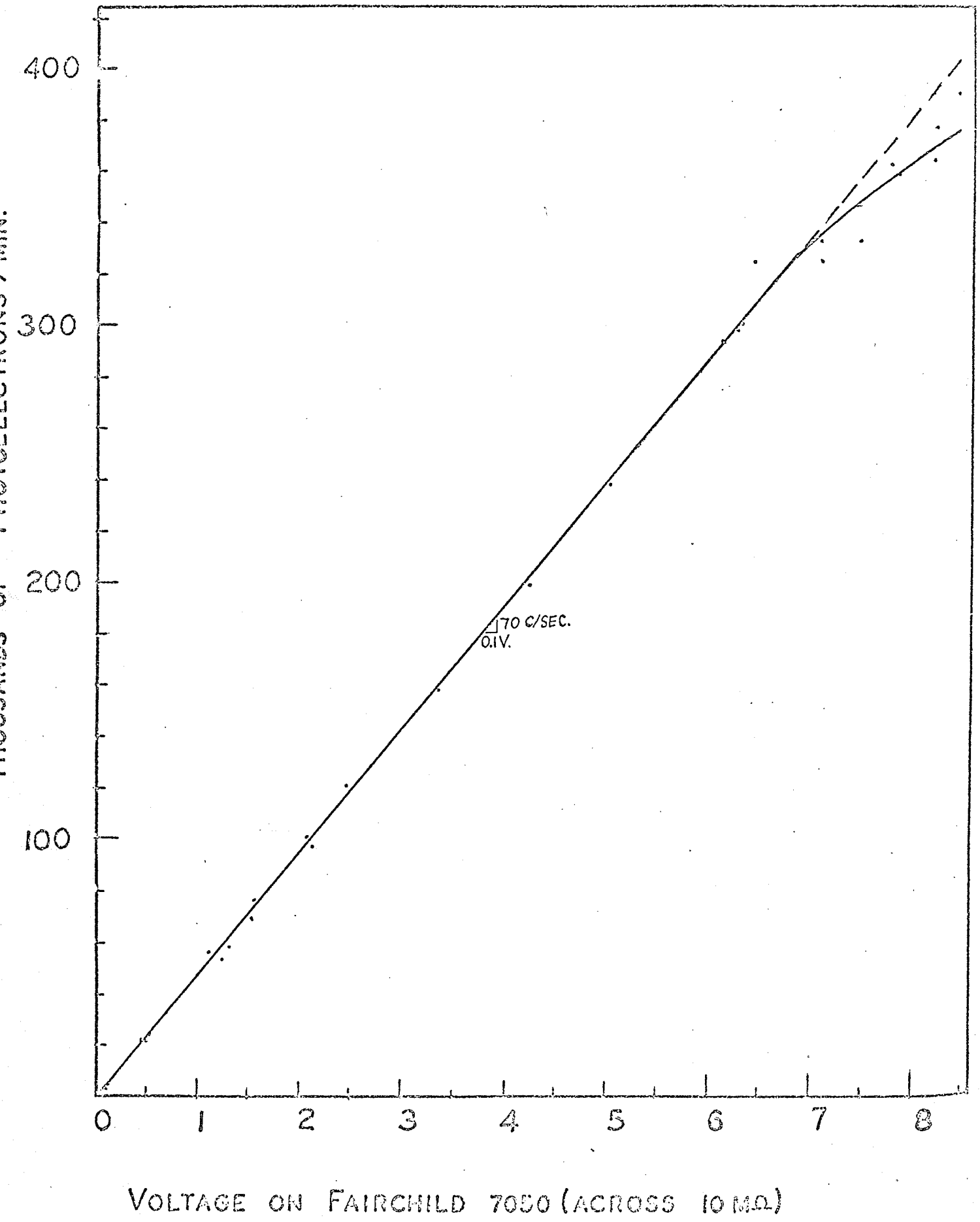
400
300
200
100
0
1
2
3
4
5
6
7
8
70 C/SEC.
0.1V.
VOLTAGE ON FAIRCHILD 7050 (ACROSS 10 MΩ)

itself. For these high intensities, the deadtimes of the SCA and scaler cause the measured intensity to be low. Therefore, in the course of taking the spectral data, the intensity was kept well below the above-mentioned intensity to avoid the necessity of correcting for the deadtime of the counting system.

Conduction Crystat

The helium cryostat used in this investigation is shown in figure 3. The temperature of the crystal in the cryostat was varied from 7.8°K to 40°K by changing the pressure of the helium gas in the conduction cell. At lower pressures, the helium gas conducts less heat away from the crystal. Thus when thermal equilibrium is established a few minutes after a pressure reduction, there is a higher crystal temperature. Once filled with liquid helium, the cryostat could be expected to keep the crystal at a constant temperature for 4 to 6 hours, after which the crystal temperature started to drift slowly upward.

The temperature measurements were made with two thermistors (Keystone Type LO 904 - 180K - H - T2 and LO 904 - 3 MEG - HE - T2) which were glued with epoxy resin to the top of the crystal holder. The thermistor resistances were measured with a Fluke 7050 digital multimeter and the temperature taken from a calibration curve supplied by Keystone.

The crystal was mounted in the cryostat in such a way that the exciting radiation was incident normally onto one face of the rectangular crystal and the emitted radiation was observed in the plane of the illuminated face, at right angles to the incident radiation.

Spectral Measurements

The equipment used to measure the luminescent spectra is shown in figure 4.

The excitation monochromator used was a Bausch and Lomb high intensity .25 m monochromator containing a 2700 groove/mm grating with a 250 nm blaze. The band pass of the monochromator was set at 13.2 nm. A 45W deuterium lamp supplied by Bausch and Lomb for use with the monochromator was used as the light source. The light output from the exciting monochromator was focused at normal incidence onto the crystal by the

Figure 3

Conduction cryostat

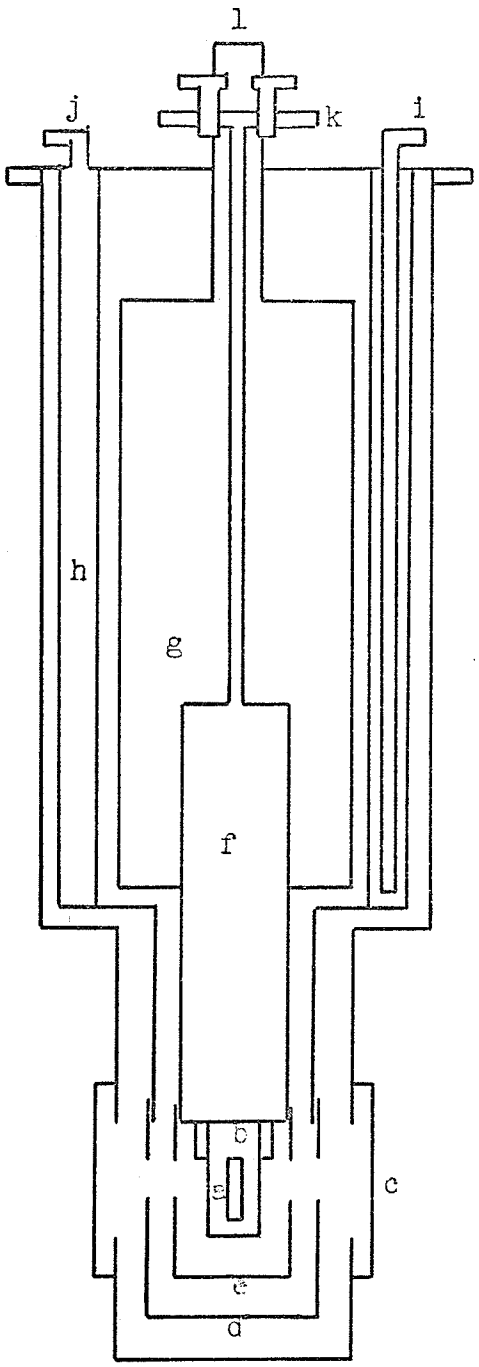

a RbCl:OH CRYSTAL
b CRYSTAL HOLDER
c QUARTZ WINDOW
d HEAT SHIELD
e HEAT SHIELD
f CONDUCTION CELL
g LIQUID HELIUM RESEVOIR
h LIQUID NITROGEN RESEVOIR
i LIQUID NITROGEN INLET
j NITROGEN VENT TUBE
k CONDUCTION CELL INLET
l LIQUID HELIUM INLET

Figure 4

Experimental arrangement of optical
and electronic equipment

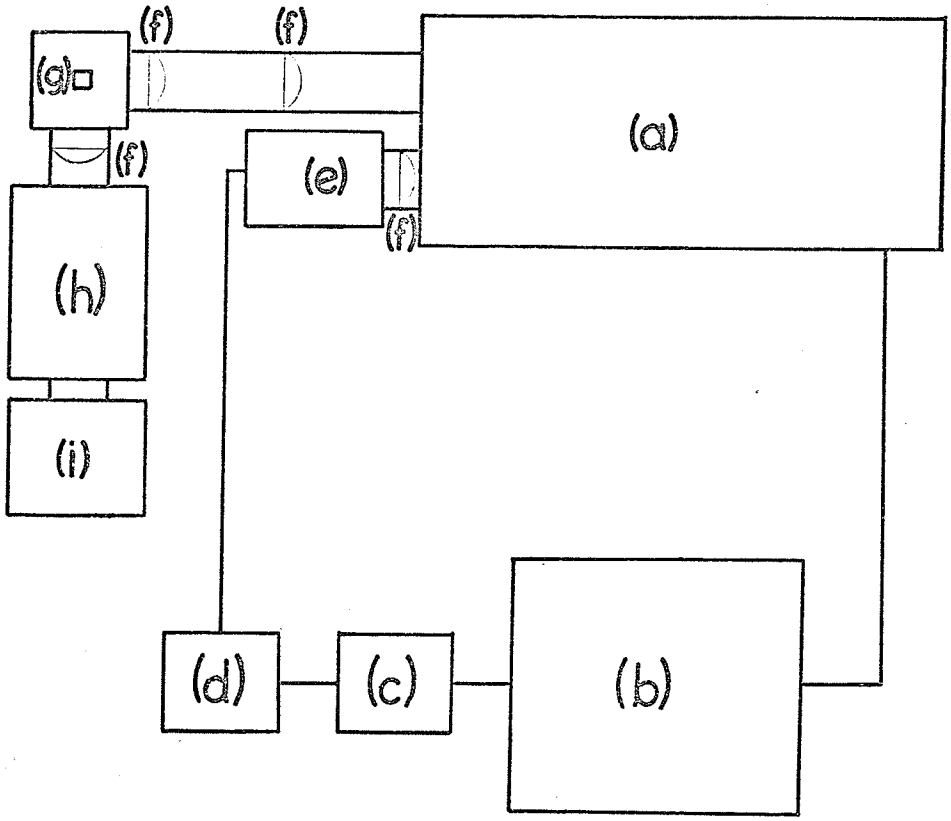

(a) SPEX MONOCHROMATOR
(b) VICTOREEN MULTICHANNEL ANALYSER
(c) SINGLE CHANNEL ANALYSER
(d) PULSE AMPLIFIER
(e) PHOTOMULTIPLIER
(f) QUARTZ LENS
(g) CRYSTAL
(h) BAUSCH AND LOMB MONOCHROMATOR
(i) BAUSCH AND LOMB DEUTERIUM LAMP

collimator lens attached to the monochromator and the lens on the cryostat. The light emitted from the crystal face was focussed onto the input slit of the emission monochromator by the two lenses shown in figure 4.

The emission monochromator used was a 1700 III Spex .75 m monochromator with a 600 grooves/mm grating blazed for 300 nm. The photomultiplier used at the output of the Spex monochromator was an EMI 6256S which was operated at 1900 volts giving a sensitivity of 5,000 amps/lumen.

The emission spectra were taken by counting the anode pulses from the photomultiplier anode on the multichannel analyser (MCA)(Victoreen Model ST400M). The channel advance pulse used to initiate the photoelectron counting in the next channel of the MCA was supplied by a circuit in the Spex monochromator. Thus the counting channel was advanced every 1.0 nm. The Spex monochromator was set for a band pass of 1.1 nm. However, due to the scanning process taking place while the MCA was counting in each channel, the effective band pass is increased to 2.1 nm.

The excitation spectra were taken by scanning the Bausch and Lomb monochromator and advancing the MCA with an external scaler at 3.42 seconds per channel which is 0.77 nm per channel.

Calibration

Both the Spex and the Bausch and Lomb monochromators were calibrated in wavelength by measuring the line spectrum of a mercury light source. The Spex monochromator was calibrated with the light source illuminating the input slit through the cryostat optics system. The Bausch and Lomb monochromator was fitted with a 1P28 photomultiplier and the mercury source was set so that it illuminated the input slit. At a later stage it was found necessary to check the calibration of the drive on the exciting monochromator thus calibration of the Bausch and Lomb monochromator was additionally performed by mea-

suring the continuous spectrum of a deuterium light source with an interference filter in front of the input slit.

The intensity calibrations were performed previously, as described by Palser (PHD Thesis 1969, University of Manitoba). The computer programs used to correct the data and convert the spectra from a linear wavelength scale to a linear energy scale were supplied by R. Palser. The raw spectral data for these programs were linear in wavelength. These programs converted this to a linear energy scale and corrected the emission spectral data for the sensitivity of the system at different wavelengths and the excitation spectral data for the intensity output as a function of wavelength. In the course of the conversion to a linear wavelength scale, some smoothing of the spectral data was necessary.

CHAPTER III

THE CONFIGURATION COORDINATE MODEL

The configurational coordinate diagram is essentially a diagram of total energy of the luminescent centre versus the configurational coordinate. This coordinate is based on the assumption that centres are sensitive to some single vibrational mode. Typically this is the "breathing mode", which is the motion of nearest neighbours toward and away from the luminescent impurity centre. Thus the configurational coordinate is normally the distance from the centre atom to the nearest neighbour. The total energy in the configuration coordinate diagram figure 5, represents the ionic and electronic energy of the ground and excited states of the luminescent centre.

The luminescent centre obeys the Frank-Condon principle which states that an electronic transition takes place in a short time compared to the vibrational mode time period of the ions. For this reason, when a photon of energy E_{AB} is absorbed while the centre is in the equilibrium position of the ground state at A, the transition is a vertical one to B as shown. The centre then moves to its new equilibrium energy at C, the energy, E_o, being given off as lattice vibrations or phonons. The excited centre may then undergo a transition back to the ground state, going from C vertically down to D, emitting a photon of energy E_{CD}. Then the centre returns to its equilibrium position A, giving up more energy to the lattice. Thus one can see immediately that this model explains the Stokes

Figure 5

Configurational coordinate diagram

U_e First excited electronic state

U_{go} Ground electronic state

U_{g1} First vibrational state of the ground electronic state

U_{g2} Second vibrational state of the ground electronic state

(a) IR absorption transition

(b) UV emission transitions

(c) UV absorption transitions

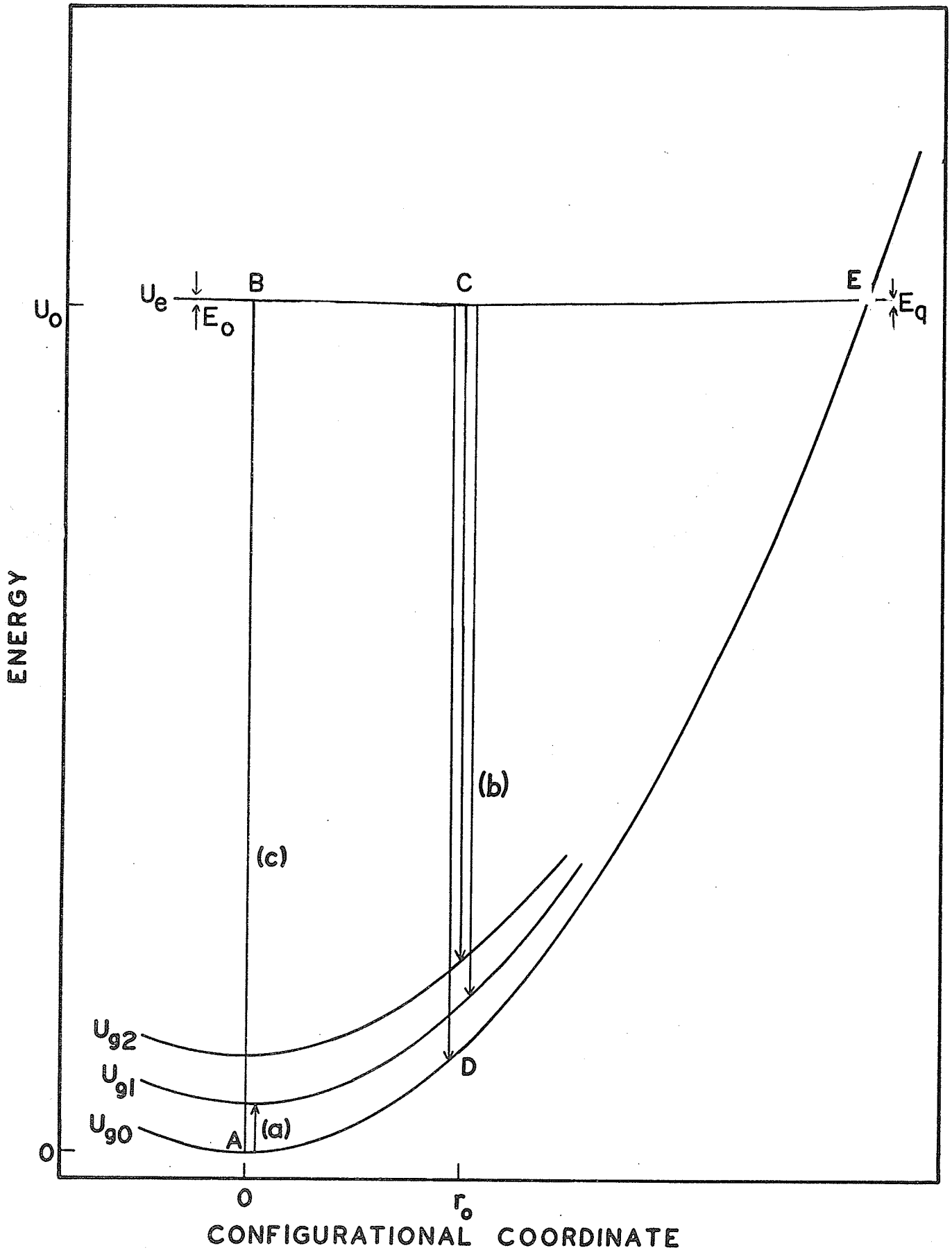
U_e
E_o
B
C
E
E_q
U_o
ENERGY
(b)
(c)
U_{g2}
U_{g1}
U_{g0}
D
A
(a)
0
0
r_o
CONFIGURATIONAL COORDINATE

shift exhibited by luminescent centres. The Stokes shift is the energy decrease of the emitted light compared to the energy of the absorbed light due to the energy given up to the lattice.

If the excited centre has enough thermal energy at C to reach E, then it can immediately go to the ground state without emitting a photon, and all of the energy of the absorbed photon goes into the lattice. This accounts for the sudden decrease in luminescent efficiency at high temperature. This is thermal quenching of luminescence.

The probability of this thermal process leading to a non-radiative transition is:

$$P_T = S \exp(-E_q/kT)$$

Where E_q is the energy from the equilibrium position of the excited state to the transition point E in the configuration coordinate diagram, figure 5. If the probability of luminescence of a centre is given by P_L, the efficiency of luminescence is then

$$N = P_L/(P_L + P_T)$$

and,

$$N = \left[1 + (S/P_L) \exp(-E_q/kT) \right]^{-1} \qquad (A)$$

This equation will be useful in Chapter IV.

The shape of the emission peak must be analysed quantum mechanically in order to derive a theoretical expression for the temperature variation of the full width at half maximum.

The light intensity for electric dipole radiation is given by

$$I(h\nu_{nm}) = \frac{64\pi^4 \nu_{nm}}{3c^3} \left| \mu_{nm} \right|^2 \qquad (1)$$

for a transition from the n^{th} vibrational state of the excited state to the m^{th} vibrational state of the ground electronic state. Where μ_{nm} is the matrix element for this transition, and c is the velocity of light,

ν is the photon frequency and h is plank's constant.

If x is the electronic coordinate and r the configuration coordinate of the ions and the wave functions are separated into electronic and vibrational parts $\phi(x)$ and $\psi(r)$ then using e for electronic charge.

$$\mu_{nm} = \int \phi^*_e(x)\ \psi^{*e}_n(\underline{r} - \underline{r}_o)\ e\ \underline{x}\ \phi_g(x)\ \psi^g_m(r)\ dx\ dr$$

where e and g refer to excited and ground states. Then the separable factor μ_{eg} is defined as

$$\mu_{eg} = \int \phi^*_e(x)\ e\ \underline{x}\ \phi_g(x)\ dx$$

Since μ_{eg} depends only on the electronic states e and g, it is considered constant and then,

$$\mu_{nm} = \mu_{eg} \int \psi^{*e}_n\ (r - r_o)\ \psi^g_m(r)\ dr \qquad (2)$$

Referring to the configurational coordinate diagram figure 5, the fact that U_e and U_g are parabolic is used. Thus this is a classical picture of harmonic oscillators:

$$U^g(r) = \tfrac{1}{2} k_g r^2 \quad ; \quad U^e(r) = \tfrac{1}{2} k_e (r - r_o)^2 + U_o \qquad (3)$$

Then the functions $\psi^g_m(r)$ and $\psi^e_n(r - r_o)$ are eigenfunctions of the harmonic oscillator, with the well known solutions:

$$\psi^g_m(r) = N_m \exp\left[-\tfrac{1}{2}\left(\frac{r}{a_g}\right)^2\right] H_m\left(\frac{r}{a_g}\right)$$

$$\psi^e_n(r - r_o) = N_n \exp\left[-\tfrac{1}{2}\left(\frac{r - r_o}{a_e}\right)^2\right] H_n\left(\frac{r - r_o}{a_e}\right) \qquad (4)$$

where H_m and H_n are hermite polynomials

N_n and N_m are normalization factors

and a_g and a_e are classical amplitudes of zero-point vibration

The first six hermite polynomials are given below

$$H_o = 1 \qquad H_1 = 2y$$
$$H_2 = 4y^2 - 2 \qquad H_3 = 8y^3 - 12y$$
$$H_4 = 16y^4 - 48y^2 + 12 \qquad H_5 = 32y^5 - 160y^3 + 120y$$

Note that $\exp\left[-\frac{1}{2}\ \frac{r - r_o}{a_e}\right]$ and $\exp\left[-\frac{1}{2}\ \frac{r}{a_g}^2\right]$ are gaussian about $r = r_o$ and $r = 0$ respectively so that ψ_n^e and ψ_m^g are products of gaussians with hermite polynomials. Now for a harmonic oscillator

$$\tfrac{1}{2}\ k_g\ a_g^2 = \tfrac{1}{2}\ \hbar\ \omega_g$$

and $$k_g = M\ \omega_g^2$$

Therefore

$$a_g = \sqrt{\frac{\hbar\ \omega_g}{M\ \omega_g^2}} = \sqrt{\frac{\hbar}{M\ \omega_g}}$$

Similarily $$a_e = \sqrt{\frac{\hbar}{M\ \omega_e}} \qquad (5)$$

However, M is actually an effective mass.

In general, the vibrational quantum number, m, reached after emission is high. This is true when the excited state equilibrium position is appreciably different from that in the ground state. It is not true for small r_o. Thus for high m one uses the approximation that $\left|\psi_m^g (r)\right|$ tends to the classical density distribution which has a maximum around r_m. Where r_m is given by

$$U^g (r_m) = \tfrac{1}{2}\ k_g\ r_m^2 = (m + \tfrac{1}{2})\ h\ \nu_g \qquad (6)$$

However, the initial state must be treated quantum mechanically.

For low temperatures, the emission begins from n = o, which is the only state occupied, so that

$$\mu_{om} \propto \mu_o^e \, (r_m - r_o)$$

and thus

$$\left| \mu_{om} \right|^2 \propto \exp \left[- \left(\frac{r_m - r_o}{a_e} \right)^2 \right] \qquad (7)$$

since $H_o = 1$. Thus the distribution density in the ground vibrational state is a pure gaussian. Differentiating $U^g(r)$ in region $r = r_o$

$$U^g(r_m) - U^g(r_o) = \Delta r \left[\frac{d U^g}{d r} \right]_{r = r_o}$$

$$= k_g \, r_o \, (r_m - r_o)$$

In addition

$$U^g(r_m) - U^g(r_o) = h \nu_o - h \nu_{om}$$

Combining the above two equations

$$(r_m - r_o) = \frac{h \nu_o - h \nu_{om}}{k_g \, r_o} \qquad (8)$$

This linear relationship between the energy difference and the configuration coordinate difference implies that the ground state parabola is a straight line around $r = r_o$.

Substituting equation (8) into (7) results in

$$\left| \mu_{om} \right|^2 \propto \exp \left[- \frac{(h \nu_{om} - h \nu_o)^2}{k_g^2 \, r_o^2 \, a_e^2} \right] \qquad (9)$$

Thus from the definition of a gaussian distribution, the standard deviation, σ, can be expressed as

$$2\,\sigma_e^2 = k_g^2\, r_o^2\, a_e^2 = (k_g\, r_o^2)\, k_g\, (a_e^2)$$

and since $\frac{1}{2}\, k_g\, r_o^2 = S_e\, h\, \nu_g$

and $k_g = M\, \omega_g^2$

where S_e is the mean number of phonons after the emission process with ground state phonon frequency ν_g. Then

$$\sigma_e^2 = (S_e\, h\, \nu_g)\; M\; \omega_g^2 \quad \frac{\hbar}{M\, \omega_e}$$

using equation (5) for a_e^2.

Thus

$$\sigma_e^2 = S_e \frac{(h\, \nu_g)^3}{h\, \nu_e} \qquad \text{for emission}$$

$$\sigma_a^2 = S_a \frac{(h\, \nu_e)^3}{h\, \nu_g} \qquad \text{for absorption} \tag{10}$$

and

$$\frac{\sigma_e^2}{\sigma_a^2} = \frac{S_e}{S_a} \left(\frac{\nu_g}{\nu_e}\right)^4 \tag{11}$$

When ν_g is known, it is possible to determine the parabolic constant $k_g = M\, \omega_g^2$, although there is some uncertainty about the value of M that should be used. However, this value of M is the same for excited and ground states and

$$\frac{k_g}{k_e} = \left(\frac{\omega_g}{\omega_e}\right)^2$$

The probability that the n^{th} vibrational level is occupied at temperature T, p_n, is given by the Boltzman factor. This assumes that ther-

mal equilibrium has been established. Evidence exists for KCl (Tl) from Louchtchik et al suggesting that equilibrium is established very quickly, since the luminescence quantum yield is independent of the exciting wave length, so long as it is within the absorption band.[26] Thus

$$P_n = \frac{\exp\ (-nh\ \nu_e/kT)}{\sum_{n=o} \exp\ (-nh\ \nu_e/kT)} \qquad (12)$$

Thus equation (1) is modified by P_n and

$$I\ (h\ \nu_{nm}) \propto P_n \quad \left| \psi^e_n\ (r_m - r_o) \right|^2$$

and taking the sum over n and m

$$I\ (h\ \nu) \propto \sum_n \sum_m P_n \left| \psi^e_n\ (r_m - r_o) \right|^2 \delta(E^e_n - E^g_m - h) \qquad (13)$$

Now it is assumed that the transition takes place too fast for the ions to change positions (Frank - Condon principle), and that the position of the transition to m corresponds to the position of the classical amplitude r_m as before (ie for large value of S). Thus $\delta(E^e_n - E^g_m - h\nu)$ can be replaced by

$$\delta\left[U^e\ (r_m) - U^g\ (r_m) - h\nu\right]$$

Also the sum over the final state can be replaced by an integral since the final states comprise a quasi-continuum. Then

$$I\ (h\nu) \propto \int\left[\sum_n P_n \left|\psi^e_n\ (r_m - r_o)\right|^2 \delta\left[U^e\ (r_m) - U^g\ (r_m) - h\nu\right]\right] dr_m \qquad (14)$$

To solve (14) the Mehler formula for the Slater summations of the harmonic oscillator is used:

$$\sum \frac{\exp -(n\ 1)\alpha}{\sqrt{\pi}\ 2^n\ n!} \quad H_n^2(x) \quad e^{-x2} = \frac{1}{(2\pi \sin h\alpha)^{\frac{1}{2}}}$$

$$\exp\left(-x^2 \tanh \frac{\alpha}{2}\right) \qquad (15)$$

Writing $\alpha = \frac{h\ \nu_e}{kT}$ and $x = \frac{r_m - r_o}{a_e}$ in (15)

$$I(h\nu) \propto \int \exp\left[-\left(\frac{r_m - r_a}{a_e}\right) \tanh \left(\frac{h\ \nu_e}{2kT}\right)\right] \delta\left[U^e(r_m) - U^g(r_m) - h\nu\right] dr_m$$

For the purpose of integration

$$y = U^e(r_m) - U^g(r_m)$$

is defined and

$$d\,r_m = \frac{dr_m}{dy}\ dy \qquad (16)$$

and $\frac{1}{2} k_e a_e^2 = \frac{1}{2} \hbar\ \omega_e = \frac{1}{2} h\ \nu_e$

then

$$I(h\nu) \propto \int \exp\left[-\tfrac{1}{2} k_e (r_m - r_e)^2 \frac{2}{h\nu_e} \tanh\left(\frac{h\nu_e}{2kT}\right)\right] \delta(y - h\nu) \frac{dr_m}{dy}\ dy$$

Thus

$$I(h\nu) \propto \left(\exp\left[-\tfrac{1}{2} k_e (r - r_o)^2 \frac{2}{h\nu_e} \tanh\left(\frac{h\nu_e}{2kT}\right)\right] \frac{dr}{dy}\right)_{y = h\nu} \qquad (17)$$

Now $\left(\frac{dr}{dy}\right)_{y=h\nu}$ is the inverse rate of divergence of the parabolas U^g and U^e as a function of the configuration coordinate. If $\frac{dr}{dy}$ is linear, the band shape is pure gaussian, otherwise it is asymmetrical.

At high temperatures,

$$\frac{h\,\nu_e}{2kT} \longrightarrow 0 \quad \text{and} \quad \tanh\left(\frac{h\,\nu_e}{2kT}\right) \longrightarrow \frac{h\,\nu_e}{2kT}$$

Thus

$$I(h\nu) \propto \exp\left(-\tfrac{1}{2} k_e (r - r_o)^2/kT\right) \frac{dr}{dy} \tag{18}$$

At low temperatures, say as $T \longrightarrow 0$

$$\tanh\left(\frac{h\,\nu_e}{2kT}\right) \longrightarrow 1$$

and the low temperature expression equation (7) is arrived at.

Finally, the width L varies with temperature and by comparing (17) with a gaussian distribution it is evident that

$$L \propto \sigma \propto \left[\tanh\left(\frac{h\,\nu_e}{2kT}\right)\right]^{+\frac{1}{2}}$$

Thus

$$L_e(T) = L_e(0)\left[\tanh\left(\frac{h\,\nu_e}{2kT}\right)\right]^{\frac{1}{2}} \text{ for emission} \tag{19}$$

$$\text{and} \quad L_a(T) = L_a(0)\left[\tanh\left(\frac{h\,\nu_a}{2kT}\right)\right]^{\frac{1}{2}} \text{ for absorption}$$

At high temperatures this becomes

$$L \propto T^{\frac{1}{2}}$$

The results of this discussion of the configurational coordinate model will be used later. It will be shown that it explains a number of characteristics of the OH^- luminescence in RbCl.

CHAPTER IV

EXPERIMENTAL RESULTS

Emission Spectra

A typical emission spectrum at liquid helium temperature is shown in figure 6. The first band at 4.067 ev. is interpreted as a transition from the first excited electronic state to the ground electronic state. The second band at 3.650 ev. is due to a transition from the first electronic excited state to the first vibrational excited state of the ground electronic state. The third band at 3.24 ev. is due to a transition to the second vibrational state of the ground electronic state. These states are shown in figure 5 of the configurational coordinate model.

Table 1 shows the full width at half maximum at various temperatures. Each width measurement is an average of from one to four spectral measurements. The errors in each observation of the width of the main peak at 4.07 ev., first vibrational peak at 3.66 ev., and the second vibrational peak at 3.26 ev. are 0.004 ev., 0.006 ev., and 0.015 ev. respectively. These errors were arrived at by using the error in estimating the height of the peak from a graph to compute the error in estimating the half maximum position. From this, the error in measuring the full width at half maximum on the graph was calculated, accounting for the precision of the length measurement. The errors in the averaged values in table 1 were calculated as described by R. T. Birge.[27] He suggests that the probable error, r, in an average of a series of n measurements is calculated with the following formula:

Figure 6

Emission Spectrum of RbCl:OH at 10°K

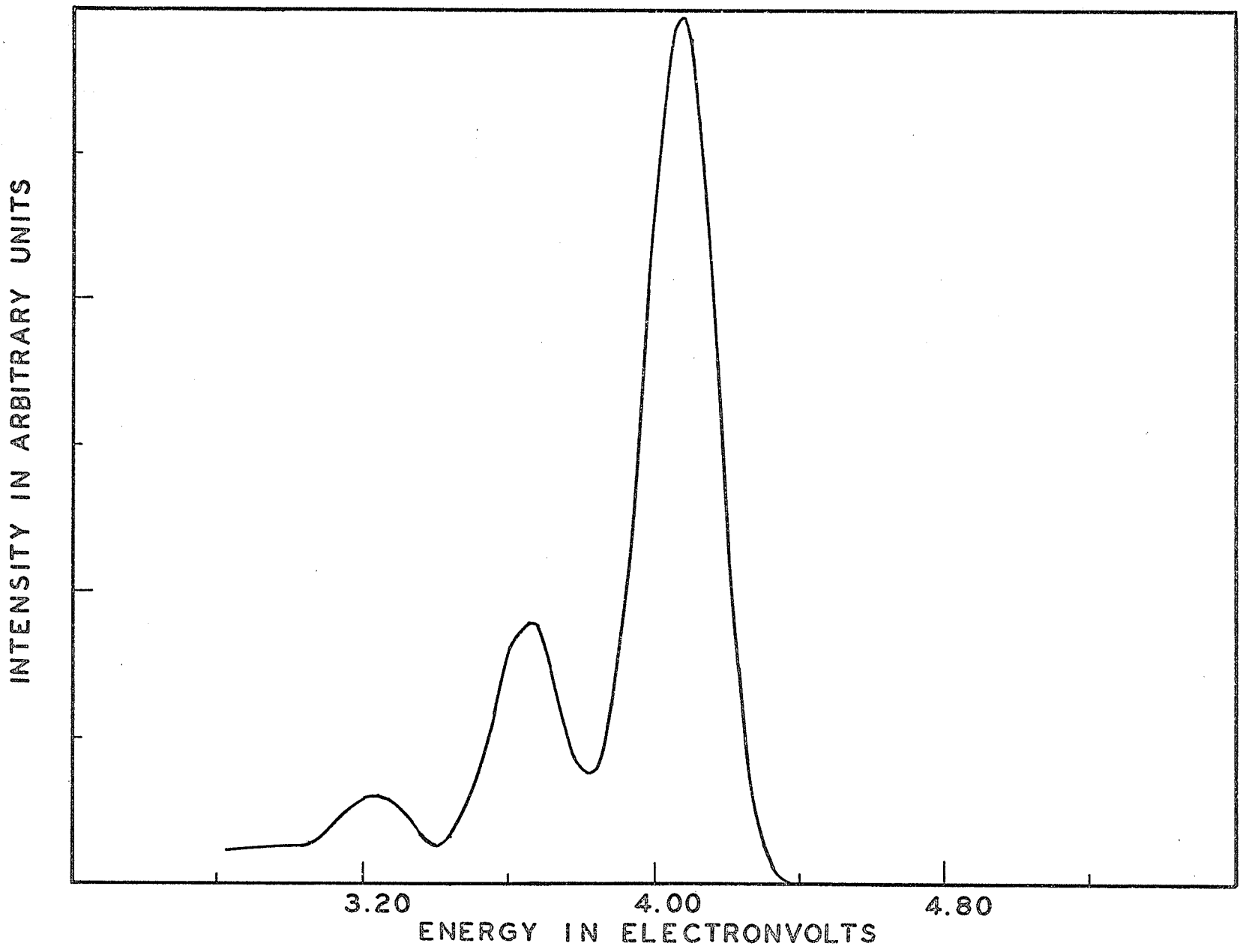
INTENSITY IN ARBITRARY UNITS
3.20
4.00
4.80
ENERGY IN ELECTRONVOLTS

$$r = 0.6745\left[\frac{Pv^2}{(n-1)(\sum P)}\right]^{\frac{1}{2}}$$

Where P is the weight of an observation calculated by taking the inverse of the error in that observation and v is the difference between that observation and the average.

The peak intensity of the third band is 6% that of the main band. Thus the fractional statistical error in this band is much larger than that for the other two bands. This statistical error leads to a large error in determining the peak height. Since the half maximum positions were found from the peak height, they have a proportionately large error associated with them. In addition, the second peak overlaps enough so that it makes a large contribution to the intensity of the higher energy half maximum position. This contribution cannot be estimated very accurately since these emission peaks are too asymmetrical. It was found that for spectra taken under similar conditions the full width at half maximum of the third band varied from 0.19 ev to 0.250 ev although in all other respects they were in agreement. The overlap of the main with the second peak was used for the second peak widths.

The peak widths of the main emission band from table 1 were fitted by applying nonlinear weighted least squares techniques (a program from the Watfiv scientific subroutine pack) to the formula

$$L_e(T) = L_e(0)\left(\text{Coth}\ \frac{h\nu_e}{kT}\right)^{\frac{1}{2}}$$

which was derived in chapter III from the configurational coordinate model. The values of $L_e(0)$ and ν_e from the fit are 0.238 ± .002 ev and (7.6 ± .2) x 10^{11} $sec.^{-1}$ respectively. Figure 7 shows the widths of the first and second emission peak from table 1 and the values of the widths at various temperatures. The widths of the second emission band at 3.66 ev have the same functional dependence on temperature as the main emission band within experimental accuracy.

TABLE 1

Width of the 4.07 ev emission band and 3.66 ev emission band at various temperatures.

Temperature ^{o}K	Full width at half maximum 4.07 ev emission	3.66 ev emission
9.1	.238 ± .002	.238 ± .004
9.3	.238 ± .003	.234 ± .014
10.1	.240 ± .008	.238 ± .006
10.8	.241 ± .002	.239 ± .004
11.2	.240 ± .002	.238 ± .003
12.6	.239 ± .004	.239 ± .003
14.1	.239 ± .003	.244 ± .014
15.8	.236 ± .004	.240 ± .006
16.3	.236 ± .004	.240 ± .006
17.2	.240 ± .001	.233 ± .011
18.0	.240 ± .004	.240 ± .006
19.3	.242 ± .005	.240 ± .004
21.9	.247 ± .008	.254 ± .004
26.0	.251 ± .004	.258 ± .006
29.5	.259 ± .009	.265 ± .006
34.5	.270 ± .009	.268 ± .010
38.0	.276 ± .004	.260 ± .006

The errors in each observation of the main, the second and third emission peak energies which were calculated in a similar fashion to the error in the widths and are ± .002 ev, ± .003 ev and ± .008 ev. The vibrational energy levels were calculated from the energy difference between the peak energies of the three emission bands. Thus the absolute errors associated with each observation of the energy of the first and second vibrational electronic states above the ground electronic state are ± .005 ev and ± 0.011 ev. Although vibrational energies reported in table 2 for various temperatures seem to have a definite shift to lower energies with higher temperature, the cumulative errors from the two emission peak positions for each make this variation difficult to analyse accurately.

The most probable peak energies of the emission bands calculated by averaging the observations of the energies of each band from all spectra are 4.073 ± .002 ev, 3.661 ± .005 ev and 3.263 ± .026 ev. These values for the band energies in RbCl:OH^- of 4.09, 3.68 and 3.28 ev reported by Köstlin.[24] It is assumed that Köstlin's measurements for RbCl:OH^- are only within 0.01 ev since he reports results with four significant figures for KI, KBr, and KCl and only three significant figures for RbCl. The most probable values of the energy difference between the first and second, and second and third emission bands, calculated by averaging each observation from each spectrum are .410 ± .003 ev and .40 ± .02 ev. These energies correspond to the energies of the first and second vibrational states above the ground electronic state. These values are essentially the same as those reported by Köstlin.[24] The energy of the first vibrational state should correspond to the value reported for the OH^- stretching band in the IR of .450 ev reported by Klein and Wedding.[8] The difference in energy between this

and the first vibrational state energy measured by uv emission suggests that the parabola used to describe this energy level in the configurational coordinate model should have a different parabolic constant than the parabola describing the ground electronic state. Thus the configurational coordinate diagram figure 5 has been drawn accordingly.

Figure 7

Functional variation of the main emission band width with temperature

· Main emission band

x First vibrational band

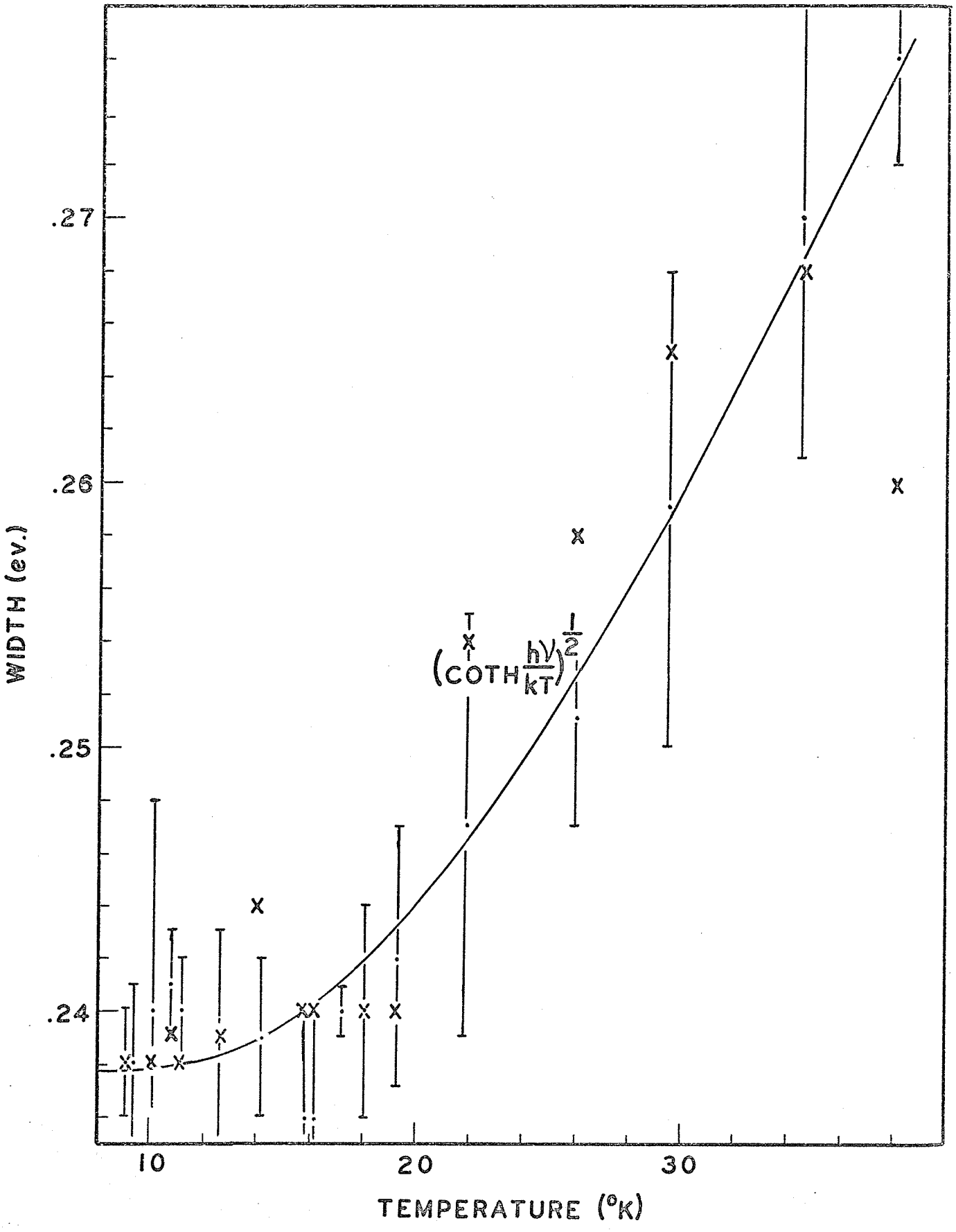
.27
.26
.25
.24
WIDTH (ev.)
10
20
30
TEMPERATURE (°K)
$(\coth \frac{h\nu}{kT})^{\frac{1}{2}}$

The areas of the emission peaks are proportional to the respective probability of the transition from the excited electronic state to one of the vibrational levels of the ground electronic state. The average ratio of the peak areas, and thus the emission probabilities are 1000: 270: 60. This ratio showed no measurable temperature variation within experimental error. This suggests that these emission peaks are due to the same electronic transition. However, the absolute areas of the emission peaks do have a temperature dependence as shown in figure 8. This figure is a graph of the logarithm of the peak area versus the inverse of the temperature for the emission peaks corresponding to transitions from the excited electronic state to the ground and first vibrational levels of the ground electronic state. The temperature dependence shown in figure 8 has the same form as that for the luminescent efficiency, N, at high temperatures as given in equation (A) in Chapter III.

Thus

$$N \propto \exp \frac{E_q}{kT} \qquad \text{and } Eq = \ln \left(\frac{N\ (T_1)}{N\ (T_2)} \right) \left(\frac{1}{T_1} - \frac{1}{T_2} \right)^{-1}$$

Values of E_q of $(2.2 \pm 0.5) \times 10^{-3}$ ev and $(2.3 \pm 0.5) \times 10^{-3}$ ev were calculated from the slopes of curves A and B respectively in Figure 8.

Excitation Spectra

A typical excitation spectrum is shown in Figure 9. The error in determining the peak energy of the excitation band is due to the inaccuracy of the Bausch and Lomb monochromator. The precision in determining the wavelength is ± 1 nm. At the excitation peak of RbCl:CH^-, this corresponds

TABLE 2

Energy differences between first and second vibrational states of excited electronic state and the zero vibrational state of the excited electronic state.

Temperature ^{o}K	Energy (ev) First vibrational state			Second vibrational state		
9.1	.416	±	.031	.410	±	.039
9.3	.415	±	.008	.405	±	.045
10.1	.413	±	.002	.404	±	.015
10.8	.414	±	.013	.397	±	.027
11.2	.413	±	.009	.404	±	.016
12.6	.412	±	.009	.405	±	.012
14.1	.412	±	.004	.398	±	.011
15.8	.400	±	.005	.412	±	.011
16.3	.413	±	.005	.386	±	.011
17.2	.414	±	.005	.394	±	.012
18.0	.417	±	.005	.398	±	.011
19.3	.399	±	.002	.394	±	.037
21.7	.407	±	.006	.395	±	.030
26.0	.406	±	.005	.382	±	.011
29.5	.410	±	.012			
34.5	.410	±	.029	.398	±	.011
38.0	.409	±	.005	.383	±	.011
Averages	.410	±	.003	.400	±	.021

Figure 8

a) Functional variation of the peak area of the main emission band with temperature.

b) Functional variation of the peak area of the first vibrational band with temperature.

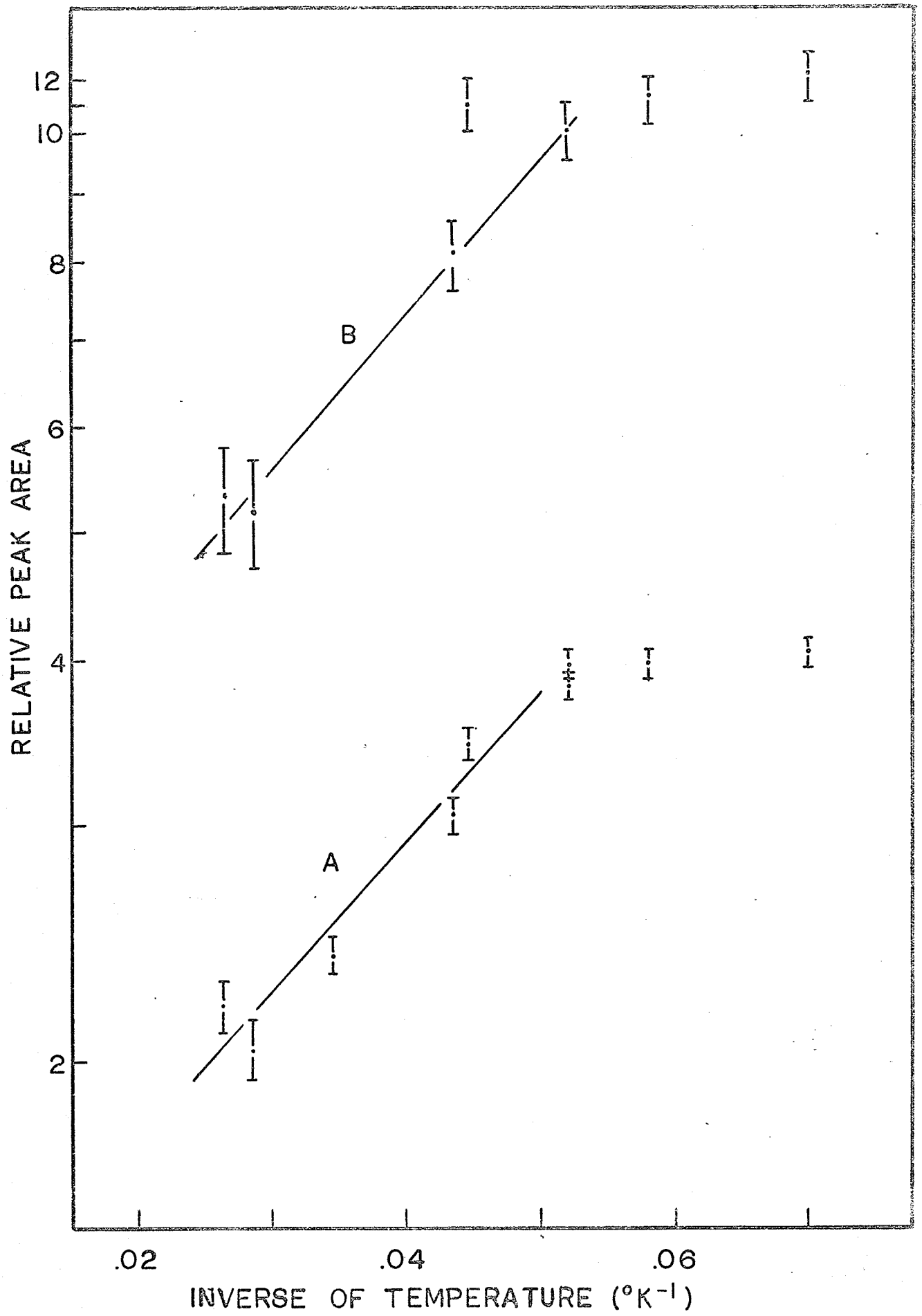
12
10
8
6
4
2
RELATIVE PEAK AREA
B
A
.02
.04
.06
INVERSE OF TEMPERATURE (°K⁻¹)

to .024 ev. This figure for the error was arrived at from a series of experiments using a 3072A° interference filter between the deuterium lamp and the monochromator and simulating an excitation experiment while measuring the output of the monochromator with an EMI 6256S photomultiplier. This showed a wavelength irreproducibility of 1 nm. The average energy of the excitation peak is 5.53 ± .03 ev and the average width is .48 ± .02 ev. This peak energy is .24 ev less than the absorption energy reported by Köstlin of 5.77 and .25 ev less than the absorption energy reported by Klein of 5.78 ev.[2,24] The errors in the measurements were too large for any functional variation of the width with temperature to be distinguished.

The excitation spectra for each emission band have the same energy peak and width within experimental error. This supports the assumption that the second and third emission peaks are due to vibrational states of the ground electronic state.

Figure 9

Excitation Spectrum of RbCl:OH at 9°K

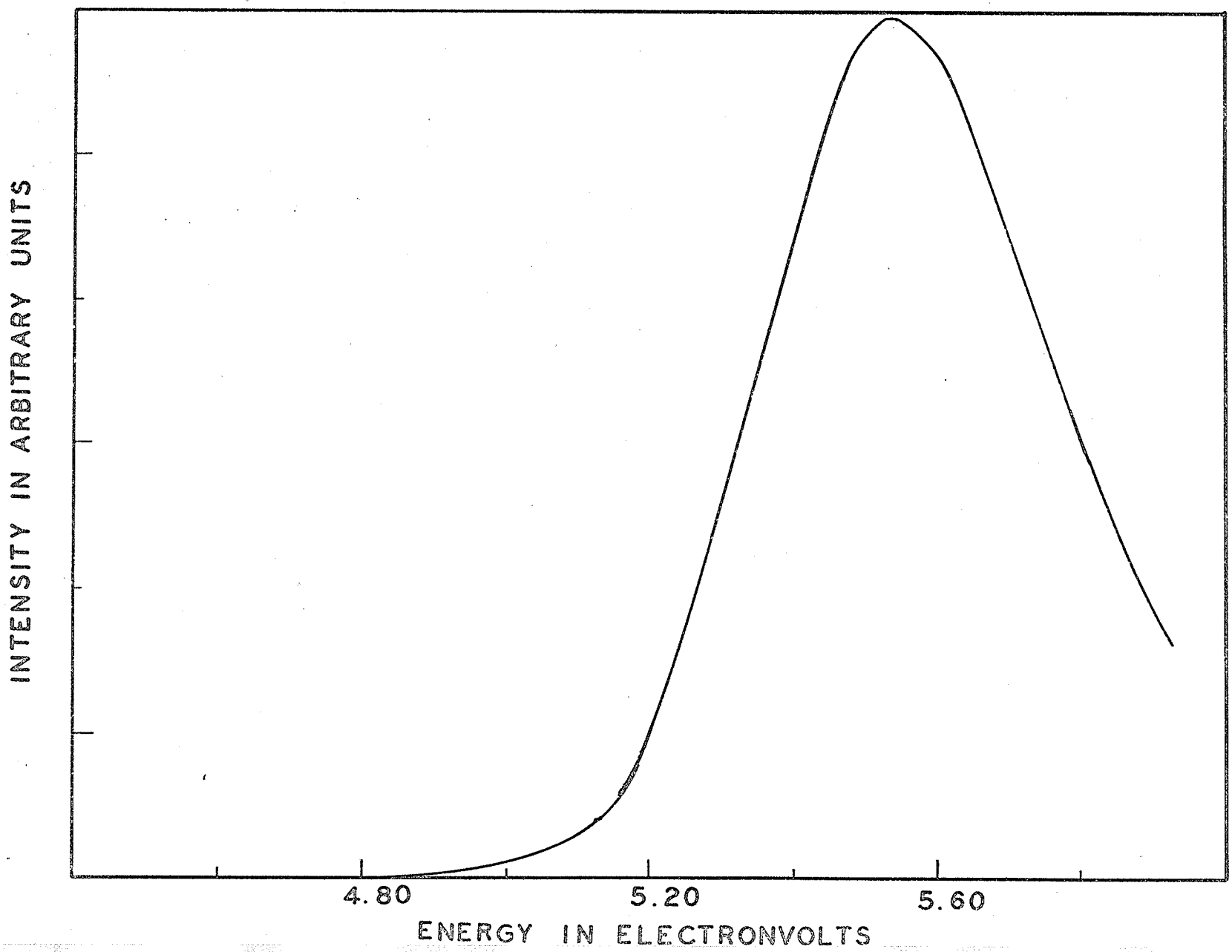
INTENSITY IN ARBITRARY UNITS
4.80
5.20
5.60
ENERGY IN ELECTRONVOLTS

CHAPTER V

CONCLUSIONS

The emission spectrum of RbCl:OH^- at liquid helium temperatures was shown to have three emission energy bands; the main energy band at 4.073 ± .002 ev, the first vibrational energy band at 3.661 ± .005 ev, and the second vibrational energy band at 3.263 ± .026 ev. Each of these results is 0.02 ev lower than those reported by Kostlin. This suggests some type of systematic error since measurement of agreement calculations predict a probability of 0.6% that each of the three pairs of measurements would differ by 0.02 ev. Since the emission monochromator used in this study had a reproducibility of .3A and a wavelength calibration was performed at the onset of this study, it is improbable that this systematic error could be attributed to this investigation.

Within experimental error, all three bands have the same excitation spectra with a peak at 5.53 ± .03 ev and a width of 0.48 ± .02 ev. This supports the assumption that these two vibrational bands are due to transitions from the excited electronic state to the first and second vibrational states of the ground electronic state.

The energy differences between the first and second vibrational states and the zero vibrational state of the excited electronic state were shown to be .410 ± .003 ev and .40 ± .02 ev respectively. This agrees with previous results in the uv although the first vibrational energy is 0.04 ev below the infrared OH^- stretching band. This difference in energy suggests that in the configurational coordinate model the parabolic constants describing the vibrational states of the ground

electronic state are different than the parabolic constant of the ground electronic state.

The width of the main peak was shown to vary with temperature with a functional variation predicted by the configurational coordinate model

$$L_e(T) = L_e(0) \left(\tanh \frac{h \nu_e}{kT} \right)^{\frac{1}{2}}$$

The vibrational frequency of the phonons emitted after the transition to the ground state, ν_e, was found to be $(7.6 \pm .2) \times 10^{11}$ sec^{-1}. While $L_e(0)$ or the half width of $0^{\circ}K$ was shown to be $.238 \pm .002$ ev. Within experimental error the width of the first vibrational band followed the same temperature variation as the main band.

The temperature dependence of the emission peak area and thus the transition probability was found to agree with the temperature variation predicted by the configurational model. The quenching energies, E_q, of $(2.2 \pm 0.5) \times 10^{-3}$ ev and $(2.3 \pm 0.5) \times 10^{-3}$ ev were found for the main and first vibrational emission peaks.

This close agreement of the quenching energies for these two bands is to be expected if both are due to the same electronic transition and the parabolic constants describing the vibrational states in the configurational coordinate model are less than that for the ground electronic state. This implies that the vibrational energy is very small for large values of the configurational coordinate.

REFERENCES

1. S. Akpinar, Ann. Physik 37, 429 (1940).
2. M. V. Klein, S. O. Kennedy, Tan Ik Gie, and B. Wedding, Mater. Res. Bull. 3, 677 (1968).
3. U. M. Grassano and P. W. M. Jacobs, J. Appl. Phys. 35, 2391 (1964).
4. D. A. Patterson, Phys. Rev. 127, 1564 (1962).
5. T. G. Stoeb, J. Phys. Chem. Soc. 28, 1375 (1967).
6. D. A. Otterson, J. Chem. Phys. 33, 227 (1960).
7. H. W. Morgan and P. A. Staats, J. Appl. Phys. 33, 364 (1962).
8. B. Wedding and M. V. Klein, Phys. Rev. 177, 1274 (1969).
9. U. Kuhn and F. Lüty, Solid State Commun. 2, 281 (1964).
10. H. Paus and F. Lüty, Phys. Status Solidi 12, 341 (1965).
11. H. Hartel and F. Lüty, Phys. Status Solidi 12, 347 (1965).
12. B. Wedding and M. V. Klein, Bull. Am. Phys. Soc. 11, 228 (1966).
13. W. Känzig, H. R Hart, Jr., and S. Roberts, Phys. Rev. Letters 13, 543 (1964).
14. U. Kuhn and F. Lüty, Solid State Commun. 3, 31 (1965).
15. I. Shepherd, J. Phys. Chem. Sol. 28, 2027 (1967).
16. W. N. Lawless, J. Phys.Chem.Solids 28, 1755 (1967).
17. W. E. Bron and R. W. Dreyfus, Phys. Rev. Letters 163, 304 (1967).
18. H. Köstlin, Solid State Commun. 4, 81 (1965).
19. F. Lüty, J. Phys. (Paris) 28, Suppl. C-4, 120 (1967).
20. H. W. Etzel, and D. A. Patterson, Phys. Rev. 112, 1112 (1958).
21. J. Rolfe, Phys. Rev. Letters 1, 56 (1958).
22. B. Fritz, F. Lüty, and J. Anger, Z. Physik 174, 240 (1963).

23. D. A. Patterson and M. N. Kabler, Solid State Commun. 3, 75 (1965).

24. H. Köstlin, Z. Physik 204, 290 (1967).

25. M. V. Klein, B. Wedding and M. A. Levine, Phys. Rev. 180, 902, (1969).

26. Tech. B. Louchtchik, N. E. Louchtchik and K. K. Shvarts, Optics and Spectr. 9, 113 (1960).

27. R. T. Birge, Review of Modern Physics 1, 1 (1929).

BIBLIOGRAPHY

D. Curie, "Luminescence in Crystals", Methuen, London (1963).

W. B. Fowler, "Physics of Color Centers", Academic Press, New York (1968).

J. J. Markham, "F-Centers in Alkali Halides", Academic Press, New York (1966).

J. H. Schulman and W. D. Compton, "Color Centers in Solids", Macmillan, New York (1962).